We are IntechOpen,
the world's leading publisher of
Open Access books
Built by scientists, for scientists

6,900
Open access books available

185,000
International authors and editors

200M
Downloads

Our authors are among the

154
Countries delivered to

TOP 1%
most cited scientists

12.2%
Contributors from top 500 universities

CLARIVATE ANALYTICS

BOOK CITATION INDEX

INDEXED

WEB OF SCIENCE™

Selection of our books indexed in the Book Citation Index
in Web of Science™ Core Collection (BKCI)

Interested in publishing with us?
Contact book.department@intechopen.com

Numbers displayed above are based on latest data collected.
For more information visit www.intechopen.com

New Robust Obstacle Detection System using Color Stereo Vision

Iyadh Cabani, Gwenaëlle Toulminet and Abdelaziz Bensrhair
Laboratoire d'Informatique, de Traitement de l'Information et des Systèmes - EA 4051,
INSA de Rouen
Campus du Madrillet, Avenue de l'Université
76801 Saint-Etienne-du-Rouvray Cedex
France

1. Introduction

Intelligent transportation systems (ITS) are divided into intelligent infrastructure systems and intelligent vehicle systems. Intelligent vehicle systems are typically classified in three categories, namely 1) Collision Avoidance Systems; 2) Driver Assistance Systems and 3) Collision Notification Systems. Obstacle detection is one of crucial tasks for Collision Avoidance Systems and Driver Assistance Systems. Obstacle detection systems use vehicle-mounted sensors to detect obstuctions, such as other vehicles, bicyclists, pedestrians, road debris, or animals, in a vehicle's path and alert the driver.

Obstacle detection systems are proposed to help drivers see farther and therefore have more time to react to road hazards. These systems also help drivers to get a large visibility area when the visibility conditions is reduced such as night, fog, snow, rain, ...

Obstacle detection systems process data acquired from one or several sensors: radar Kruse et al. (2004), lidar Gao & Coifman (2006), monocular vision Lombardi & Zavidovique (2004), stereo vision Franke (2000) Bensrhair et al. (2002) Cabani et al. (2006b) Kogler et al. (2006) Woodfill et al. (2007), vision fused with active sensors Gern et al. (2000) Steux et al. (2002) Möbus & Kolbe (2004)Zhu et al. (2006) Alessandretti et al. (2007)Cheng et al. (2007). It is clear now that most obstacle detection systems cannot work without vision. Typically, vision-based systems consist of cameras that provide gray level images. When visibility conditions are reduced (night, fog, twilight, tunnel, snow, rain), vision systems are almost blind. Obstacle detection systems are less robust and reliable. To deal with the problem of reduced visibility conditions, infrared or color cameras can be used.

Thermal imaging cameras are initially used by militaries. Over the last few years, these systems became accessible to the commercial market, and can be found in select 2006 BMW cars. For example, vehicle headlight systems provide between 75 to 140 meters of moderate illumination; at 90 K meters per hour this means less than 4 seconds to react to hazards. When with PathFindIR *PathFindIR* (n.d.) (a commercial system), a driver can have more than 15 seconds. Other systems still in the research stage assist drivers to detect pedestrians Xu & Fujimura (2002) Broggi et al. (2004) Bertozzi et al. (2007).

Color is appropriate to various visibility conditions and various environments. In Betke et al. (2000) and Betke & Nguyen (1998), *Betke et al.* have demonstrated that the tracking of

vehicles by night, in tunnels, in rainy and snowy weather in various environment is possible with color. Recently, *Jia* Jia et al. (2007) fuses information captured by color cameras and inertial motion sensors for tracking objects. *Steux et al.* use color to recognize vehicles on highways, roads and in an urban environment Steux et al. (2002). The same approach has been used to recognize vehicles: rear lights are extracted in the RGB color space. *Daimler Chrysler* Franke et al. (1999) and *Maldonado-Bascon et al.* Maldonado-Bascon et al. (2007) use color to detect road, traffic signs and traffic signals in urban traffic environment. Recently, we have proposed a color based method to detect vehicle lights Cabani et al. (2005). The vision system detects three kinds of vehicle lights: rear lights and rear-brake-lights; flashing and warning lights; reverse lights and headlights. *Cheng et al.* Cheng et al. (2006) use color to detect lane with moving vehicles.

Initially, our laboratory has conceived a gray level stereo vision system for obstacle detection Toulminet et al. (2004) Toulminet et al. (2006) based on declivity for edges extraction Miché & Debrie (1995) and dynamic programming approach for matching Bensrhair et al. (1996). In order to improve its robustness and reliability, we currently work on the conception of a color stereo vision system for obstacle detection. The color-based approach is achieved in three main steps. In the first step, vertical edge points are extracted using the color-declivity operator. It is self-adaptive in order to face different conditions of illumination (sun; twilight; rain; fog; transition between sun and shadow; entrance or exit from a tunnel). In the second step, stereoscopic vertical edge points are matched self-adaptively using a dynamic programming algorithm. Finally, 3D edges of obstacles are detected.

The paper is organized as follows. Section 2 presents the first step of the proposed method together with color based edges segmentation methods. In section 3, the second step of our method is detailed. The state of the art of color matching is given in the first subsection. Color-based obstacle detection is depicted in section 4. Performance of each step is discussed and experimental results are shown.

2. Edge-based color image segmentation

2.1 State of the art
A lot of research has been done recently to tackle the color edge detection problem can be divided into three parts as follows Ruzon & Tomasi (2001):
- output fusion methods
- multidimensional gradient methods
- vector methods

Recently, *Macaire* Macaire (2004) takes back this classification and enriched it by a new category. This new category regroups methods based on vector gradient computed on single channel image called single channel methods.

2.1.1 Single channel methods
These methods perform the grayscale edge detection (Sobel, Prewitt, Kirsch, Robinson, etc.) on single channel. Often, luminance channel is used. These methods prove to be efficient when the levels of luminance of the pixels representing objects are enough to differentiate them.

2.1.2 Output fusion methods
Output fusion appears to be the most popular. These methods perform the grayscale edge detection on each channel and then the results are combined to produce the final edge map

using simple logical/arithmetical operations (i.e. OR Fan, Yau, Elmagarmid & Aref (2001)Fan, Aref, Hacid & Elmagarmid (2001), AND, majority-voting, a summation Heddley & Yan (1992), a weighted sum Nevatia (1977)Carron & Lambert (1994)Carron & Lambert (1995)). *Nevatia* Nevatia (1977) developed the first output fusion method, in which he extended the Hueckel operator Hueckel (1971) to color edges. *Shiozaki* Shiozaki (1986) weighted the results of his entropy operator by the relative amounts of each channel at a pixel. *Malowany* and *Malowany* Malowany & Malowany (1989) added absolute values of Laplacien outputs. *Carron* and *Lambert* computed edge strength using a weighted sum over each component in Carron & Lambert (1994) and extension using fuzzy sets in Carron & Lambert (1995) on HSI color space. *Weeks et al.* Weeks et al. (1995) combined edges found in the H, S and I components of a color image. *Alberto-Salinas et al.* Salinas et al. (1996) have proposed a more sophisticated approach. The Canny operator Canny (1986) is applied to each channel then regularization is used as a way to fuse the outputs.

2.1.3 Multidimensional gradient methods

Multidimensional gradient methods are characterized by a single estimate of the orientation and strength of an edge at a point. *Robinson* suggest to compute 24 directional derivatives (8 neighbors × 3 components) and chose the one with the highest magnitude as the gradient. The most known multidimensional gradient method have been defined by *Di Zenzo* Di-Zenzo (1986). Di Zenzo gives formulas for computing the magnitude and direction of the gradient (which, for color images, is a tensor) given the directional derivatives in each channel. A 2 × 2 matrix is formed from the outer product of the gradient vector in each component. These matrices are summed together, noted S. The square root of the principal eigenvalue represents the magnitude of the gradient. The corresponding eigenvector yields the gradient direction. Di Zenzo showed howto compute this gradient using the Sobel operator, but he did not detect edges directly. Cumani Cumani (1991) is the first to have use multidimensional gradients for detecting edges. *Chapron* Chapron (1992)Chapron (1997) used the Canny-Deriche gradient in each component. The DempsterShafer theory is used in Chapron (2000) for fusing the gradients. Others have developed distinctly different approaches. *Moghaddemzadeh* and *Bourbakis* Moghaddamzadeh & Bourbakis (1995) Moghaddamzadeh et al. (1998) used a normalized hue contrast in the HSI color space to compensate for low saturations. *Tsang* and *Tsang* Tsang & Tsang (1996) Tsang & Tsang (1997) used a heuristic choice of component gradients in HSV color space. *Macaire et al.* Macaire et al. (1996) used relaxation on the normalized Sobel gradient to classify pixels. Finally, *Scharcanski* and *Venetsanopoulos* Scharcanski & Venetsanopoulos (1997) averaged color vectors together before computing directional derivatives and a gradiant.

2.1.4 Vector methods

The first research works into vector methods has used differential geometry to determine the rate of change and corresponding direction at each pixel Chapron (1997)Zugaj & Lattuati (1998). Other research has considered the use of probability distributions. In Machuca & Phillips (1983), *Machuca* and *Phillips* defined the first vector method for color edge detection. They created onedimensional vectors, as they felt that color was useful only where grayscale edge detection failed. *Huntsberger* and *Descalzi* Huntsberger & Descalzi (1985) used fuzzy membership values. *Pietikainen* and *Harwood* Pietikainen & Harwood (1986) used histograms of vector differences. *Yang* and *Tsai* Yang & Tsai (1996) and *Tao* and *Huang* Tao & Huang

(1997) used vector projections. *Trahanias* and *Venetsanopoulos* Trahanias & Venetsanopoulos (1996) used the median of a set of vectors. *Djuric* and *Fwu* Djuric & Fwu (1997) found edges using the MAP (maximum a posteriori) rule. *Fotinos et al.* suggest the use of relative entropy as a dissimilarity measure between a local probability distribution and that of a homogenous region. *Ruzon* and *Tomasi* Ruzon & Tomasi (2001) suggest the use of color signatures generated using vector quantization. *Wen et al.* Wen et al. (2002) used a vector difference.

- Simplicity: OR operation can be easily implemented on dedicated architecture
- Real time constraint: OR operation is a fast solution which enables color-declivity to be fast also
- Binary output of declivity operation: as a logical operator, OR operator is more appropriate than arithmetic ones; note that AND operator is not appropriate for segmentation of real road scenes

Declivity is defined as a set of consecutive pixels in an image line whose amplitudes are a strictly monotonous function of their positions Miché & Debrie (1995). Let d a declivity denoted $d(x_i, x_{i+1}, w_i, A_i, X_i)$ where (see Fig. 1):

- x_i represents the coordinate of its first pixel in the image line
- x_{i+1} represents the coordinate of its last pixel in the image line
- $w_i = x_{i+1} - x_i$ represents its width
- $A_i = |I(x_{i+1}) - I(x_i)|$ represents its amplitude
- X_i represents its position in the image line and defined by:

$$X_i = \frac{\sum_{x=x_i}^{x_{i+1}-1}\left[I(x+1)-I(x)\right]^2 (x+0.5)}{\sum_{x=x_i}^{x_{i+1}-1}\left[I(x+1)-I(x)\right]^2} \tag{1}$$

where $I(x)$ indicates the gray level value of the pixel at position x.

In order to have an accurate disparity map, efficient locations of declivities are essential. The position of a declivity is calculated using the mean position of the declivity points weighted by the gradients squared. This quadratic form is well suited to irregular extended edges, i.e. spread over several pixels with a variable slope as it may result from the effect of non-filtered noise, and it enables the real position of edges to be computed with sub-pixel precision.
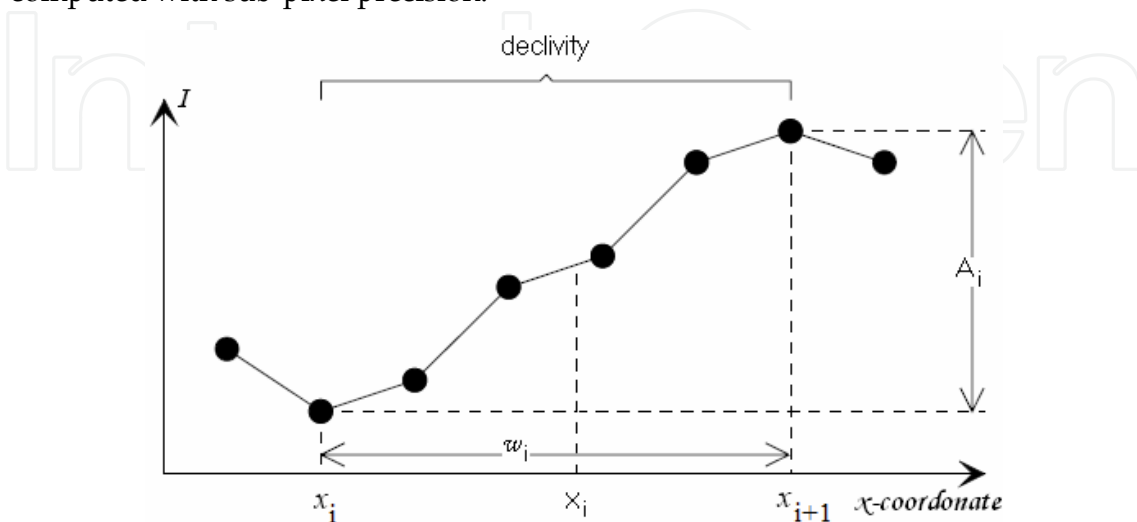

Fig. 1. Characteristics parameters of a declivity.

Declivities are independently constructed in each line of the three channels of color image. Let $D_{c \in 1,2,3}$ the set of declivities of channel c in an image line. For $d \in D_c$, the position of the declivity is noted $d(X_i)$ and its amplitude is noted $d(A_i)$. Relevant declivities (i.e. edge points) are extracted by thresholding their amplitude. Given an optimal threshold for channel c, say T_c, the E_c function, below, classifies the pixels on channel c into two opposite classes: *edge* versus *non-edge*.

$$\forall d \in D_c,$$
$$E_c(d(X_i)) = \begin{cases} 1, \text{edge pixel} & \text{if} \quad d(A_i)^2 \geq T_c^{\,2} \\ 0, \text{non-edge pixel} & \text{if} \quad d(A_i)^2 < T_c^{\,2} \end{cases} \tag{2}$$

E_c is the set of relevant declivities of channel c in an image line.

In this proposed edge detection technique, the optimal threshold T_c is self-adaptive as described in subsection 2.3. Edge results for the three color components are integrated throught the following fusion rule:

$$\forall rd \in \bigcup_{c \in [1,3]} E_c,$$
$$E(rd(X_i)) = \begin{cases} 1, \text{edge pixel} & \text{if} \quad E_1(rd(X_i)) = 1 \\ & \text{or} \quad E_2(rd(X_i)) = 1 \\ & \text{or} \quad E_3(rd(X_i)) = 1 \\ 0, \text{non-edge pixel} & \text{otherwise.} \end{cases} \tag{3}$$

The pixel is classified as the edge pixel if and only if at least one of its three color components is detected as an edge and $E(rd(X_i))$ is set to 1, otherwise, it is classified as a non-edge pixel and $E(rd(X_i))$ is set to 0. These obtained color edges can provide a simplified image that preserves the domain geometric structures and spatial relationships found in the original image.

Finally, each color-declivity is characterized by the following attributes:

- its set Ω_i which contains the numbers of channels in which declivities have been extracted. There are 8 possible sets Ω for color image. For example, $\Omega = \{1, 2,3\}$, or $\Omega = \{1,3\}$, or $\Omega = \{2\}$, ...
- the coordinate of its first pixel u_i in the color image line.

$$u_i = \max_{\forall c \in \Omega_i} \{x_{j_c}\}$$

- the coordinate of its last pixel u_{i+1} in the color image line.

$$u_{i+1} = \min_{\forall c \in \Omega_i} \{x_{j+1_c}\}$$

- its width equal to $W_i = u_{i+1} - u_i$
- its position.

The computation of u_i and u_{i+1} are obtained by maximizing, respectively minimizing the position of the first, respectively the last, pixels of relevant declivities extracted in the set of channel Ω_i. As a result monotony is observed in each channel of Ω_i.

The proposed structure of color declivity has the following advantages. It can be used for any color spaces and for any hybrid color spaces. It can also be extended to multi-spectral images.

2.3 Self-adaptive thresholding

Based on both the taxonomy of thresholding algorithms presented in Sankur & Sezgin (2004) and our previous works Miché & Debrie (1995), a self-adaptive thresholding is defined as follows:

$$T_c = \alpha \times \sigma_c \tag{4}$$

where σ_c is the standard deviation of the component of a white noise which is supposed to be Gaussian. It is deduced from the histogram of amplitude variations of pixels in an image line on channel c. In Miché & Debrie (1995), α is fixed to 5.6 for gray level image line in order to reject 99.5% of increments due to noise.

α equal to 5.6 is not appropriate for color edges segmentation, because over segmentation is observed. In Peli & Malah (1982), Pratt's figure-of-merit (FOM) is computed in order to set threshold value for edge segmentation. FOM measurement Pratt (1977) is widely used to estimate performance of edge segmentation. It is defined by:

$$FOM = \frac{1}{\max(N_I, N_D)} \sum_{i=1}^{N_D} \frac{1}{1 + ad_i^2} \tag{5}$$

where N_D is the number of detected edge points, N_I is the number of ideal edge points (ground truth), d_i is the edge deviation or error distance for the ith detected edge pixel and a is a scaling factor chosen to be $a = \frac{1}{9}$ to provide a relative penalty between smeared edges and isolated, but offset, edges. A larger value of FOM corresponds to better performance, with 1 being a perfect result.

In order to evaluate color edges segmentation and to estimate α, FOM was computed based on original Lena image (see Fig. 2) and its ideal edge map provided by experts. The best segmentation of Lena image according to FOM definition is obtained for α equal to 8 (FOM = 0.88) (see Fig. 3).
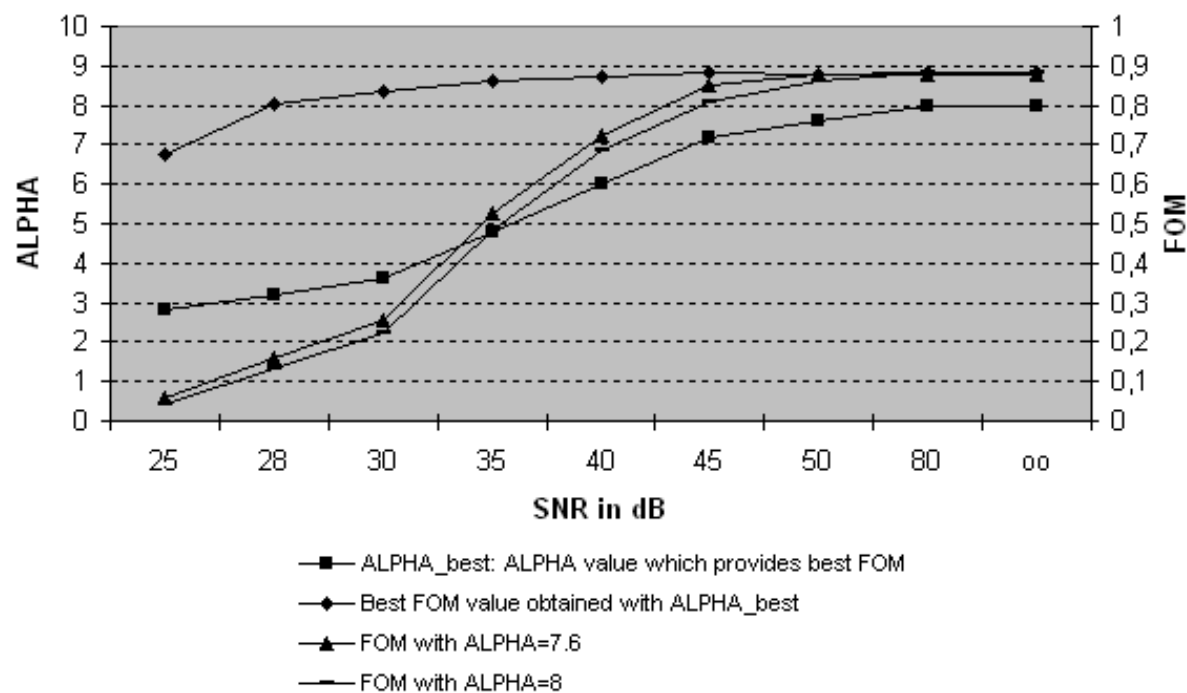

Fig. 2. Original Lena image.

Fig. 3. Three Pratt's figures-of-merit (FOM) computed with different value of α; and obtained from Lena image in which gaussian noise of different amplitude has been added $SNR \in [25,\infty[\ dB$.

Values of $\alpha \in [6.4, 9.2]$ ($FOM > 0.8$) have been studied for edge segmentation of real color images of road scenes. After many tests α was fixed to 7.6. It corresponds to rejection of 99.98% increments due to noise supposed to be gaussian in color image. In order to evaluate its noise sensitivity, color edges segmentation has been performed using Lena image in which gaussian noise of different amplitude has been added ($SNR \in [25,\infty[\ dB$). Figure 2 shows that if $SNR > 40dB$, the edges segmentation obtained with α equal to 7.6 is almost as good as the best segmentation according to definition of Pratt's figure-of-merit. Consequently, α equal to 7.6 is appropriate to standard color camera: as an example, color camera JAI CV-M91 features $SNR > 54 \ dB$.

2.4 Experimental results and discussion

For evaluating the real performance of the proposed color edge detector. It has been tested on synthetic and real road scenes. A comparison is accomplished between our color operator and the declivity operator to estimate the color improvment. For providing more convincing performance, the proposed color edge detector has been compared to variant of color Canny operator.

Fig. 4(a) shows a synthetic image consisting of three different color squares of similar intensity in a grid pattern and Fig. 5(a) shows a synthetic road scene. When a color version of the Canny operator and color-declivity operator are able to detect the borders between the squares (see Fig. 4(b) and Fig. 4(d), respectively), the declivity operator is not able to detect any edges (see Fig. 4(c)). We remark that all edges are not detected by declivity operator (Especially, border between both vehicles on Fig. 5(c)) while with color variant of Canny operator, we succeed in detecting these edges (see Fig. 5(b)). On the other hand, positions of edges detected with color variant of Canny operator are less accurate

particularly in the intersections of edges (see Fig. 4(b) and Fig. 5(b)). The color declivity succeeds in extracting edges correctly with a very good precision particularly in the case of the intersections of edges (see Fig. 4(d) and Fig. 5(d)). So we proposed a new operator for color edges detection which takes advantage of color information and advantages of declivity operator (accuracy and auto-adaptivity).

To be able to estimate the contribution of color information, we decide to push comparison between declivity operator and color-declivity operator. For this purpose, we use the Middlebury database Scharstein & Szeliski (2002). Table 1 shows that the novel approach extracts more edge points than the former one. In Fig. 7(f), edge points extracted in gray level Cones image but not in color Cones image are superimposed in color Cones image. These results can be justified by:
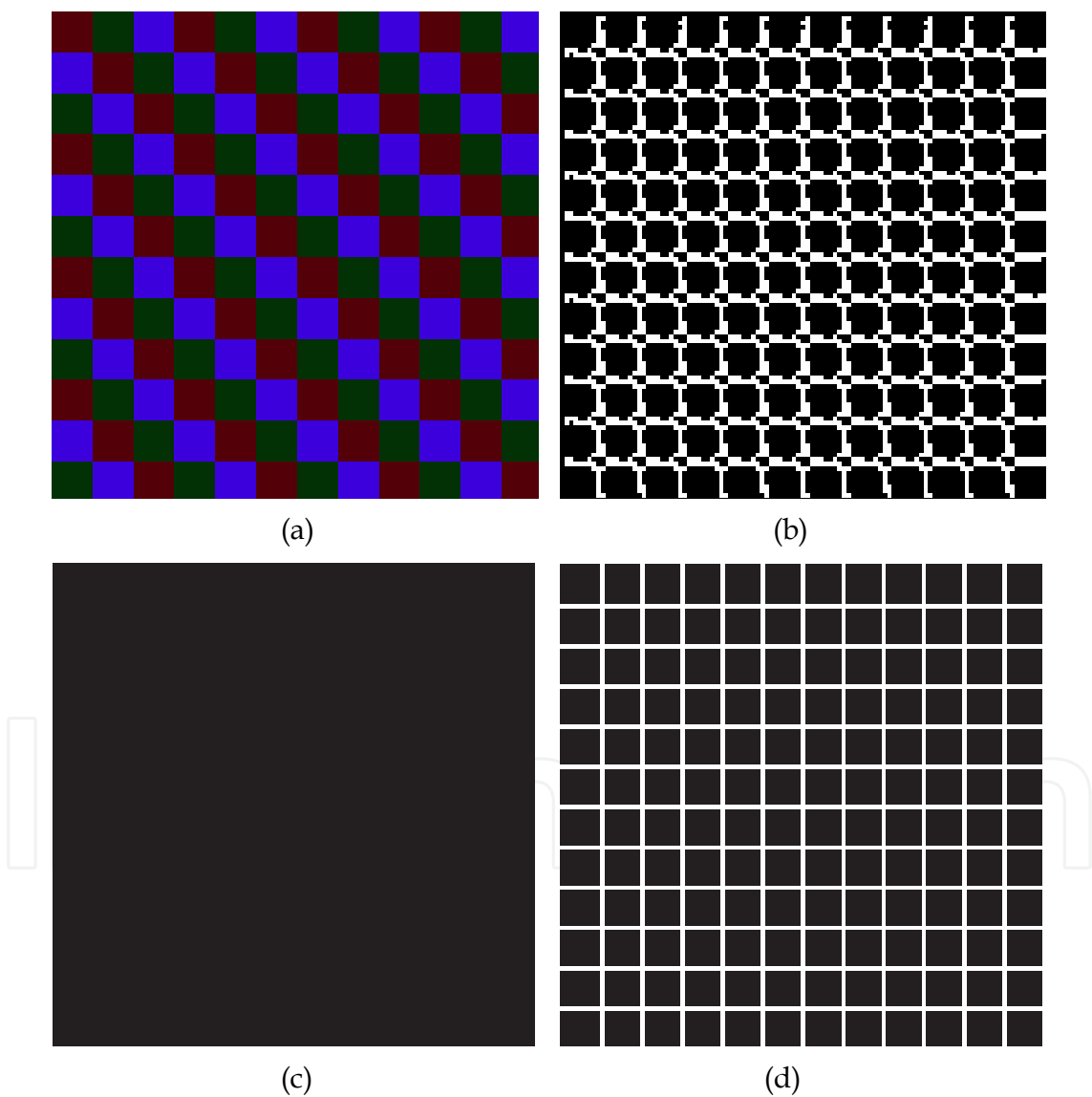

Fig. 4. Experimental results of edge detection (a) Original color image consisting of three different color squares of similar intensity in a grid pattern. (b) Results for a color variant of the Canny operator applied to the color image. (c) Results of declivity operator applied to the gray level image. (d) Results of color-declivity operator applied to the color image.
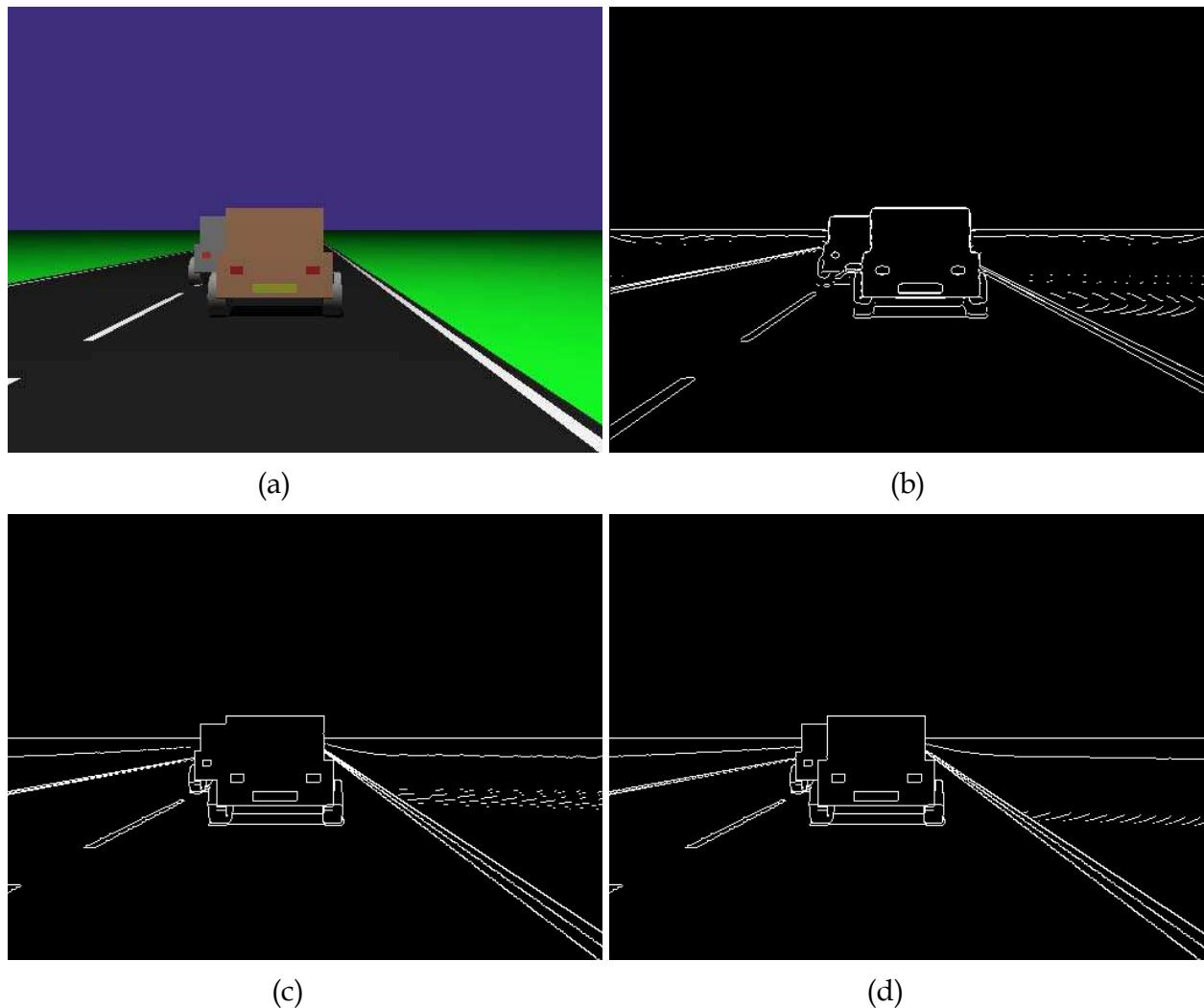
(a)

(b)

(c)

(d)

Fig. 5. Results of edge detection (a) Original color image consisting of three different color squares of similar intensity in a grid pattern. (b) Results for a color variant of the Canny operator applied to the color image. (c) Results of declivity operator applied to the gray level image. (d) Results of color-declivity operator applied to the color image.

1. Edge positions have not been correctly computed. This is due to pixels of adjacent different colored objects which feature strictly monotonous gray level values. Fig. 8 illustrates this phenomenon. In this case, two edge segments are correctly extracted using color declivity, whereas only one edge segment is extracted in gray level image. As a consequence, the position of the extracted edge segment does not correspond to position of actual edge.

2. Amplitudes of color declivity and its correspond on gray level are not the same. α is equal to 7.6 for color image and 5.6 for gray level image. The edge points extracted in gray level image but not in color image correspond to edges which have an amplitude between 5.6× σ and 7.6× σ. Infact, lower value of α for gray level image is a compromise which enables not to reject too much gray level edges and not to extract too much noise.

In Fig. 7(e), edge points extracted in color Cones image but not in gray level Cones image are superimposed in color Cones image. These edge points extracted by color-declivity are

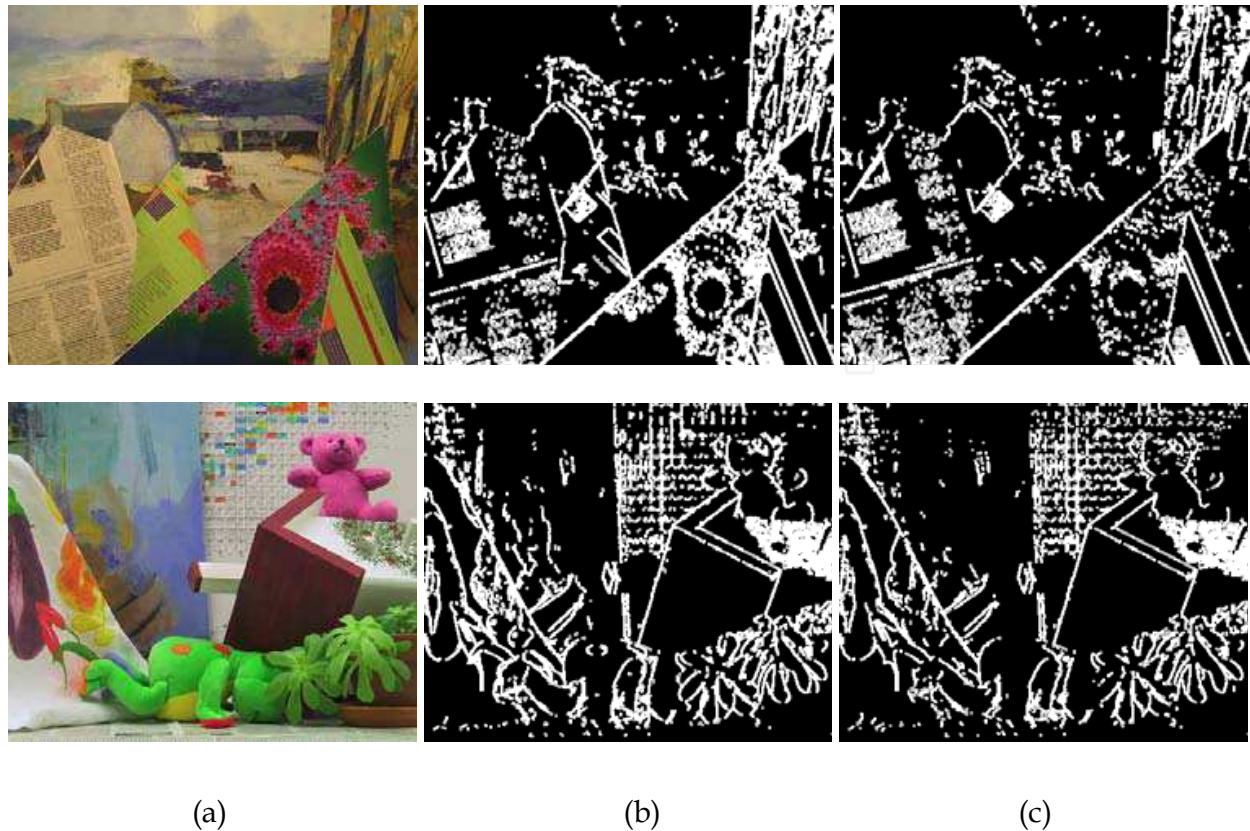(a)   (b)   (c)

Fig. 6. Experimental results of edge extraction: (a) color image (Barn 1 and Teddy). (b) color declivity image. (c) declivity image.

relevant for scene understanding. In addition to better positioning of color declivity for particular case explained in point 1., color enables to face problems of:

3. Metamerism: metamerism is observed if different colored objects reflect the same amount of light. Examples of colors which have the same gray level value in gray level image are presented in Fig. 9. Edges of adjacent different colored objects which reflect the same intensity are robustly extracted in color image, while they are not extracted in gray level image. Gray level edges segmentation problem due to metamerism is illustrated in Fig. 4. The case of the Fig. 9(b) is very interesting. We see that a shade of the red, the green and the blue be able to have an intensity in gray level equal to 127. So, the edges point separating both vehicles on the road having these colors will not be discerned by the declivity (see Fig. 5(c))

4. Adjacent different colored objects which reflect almost the same intensity: using color process, the amplitude of relevant color declivity is greater than $7.6 \times \sigma$. In this particular case, its corresponding in graylevel process have an amplitude smaller than $5.6 \times \sigma$.

As a conclusion, color edges segmentation based on color-declivity is more robust and reliable than gray level edges segmentation based on declivity. Note also that the proposed definition of color declivity can be used for any color spaces and for any hybrid color spaces. We can also extend color-declivity to multi-spectral images.
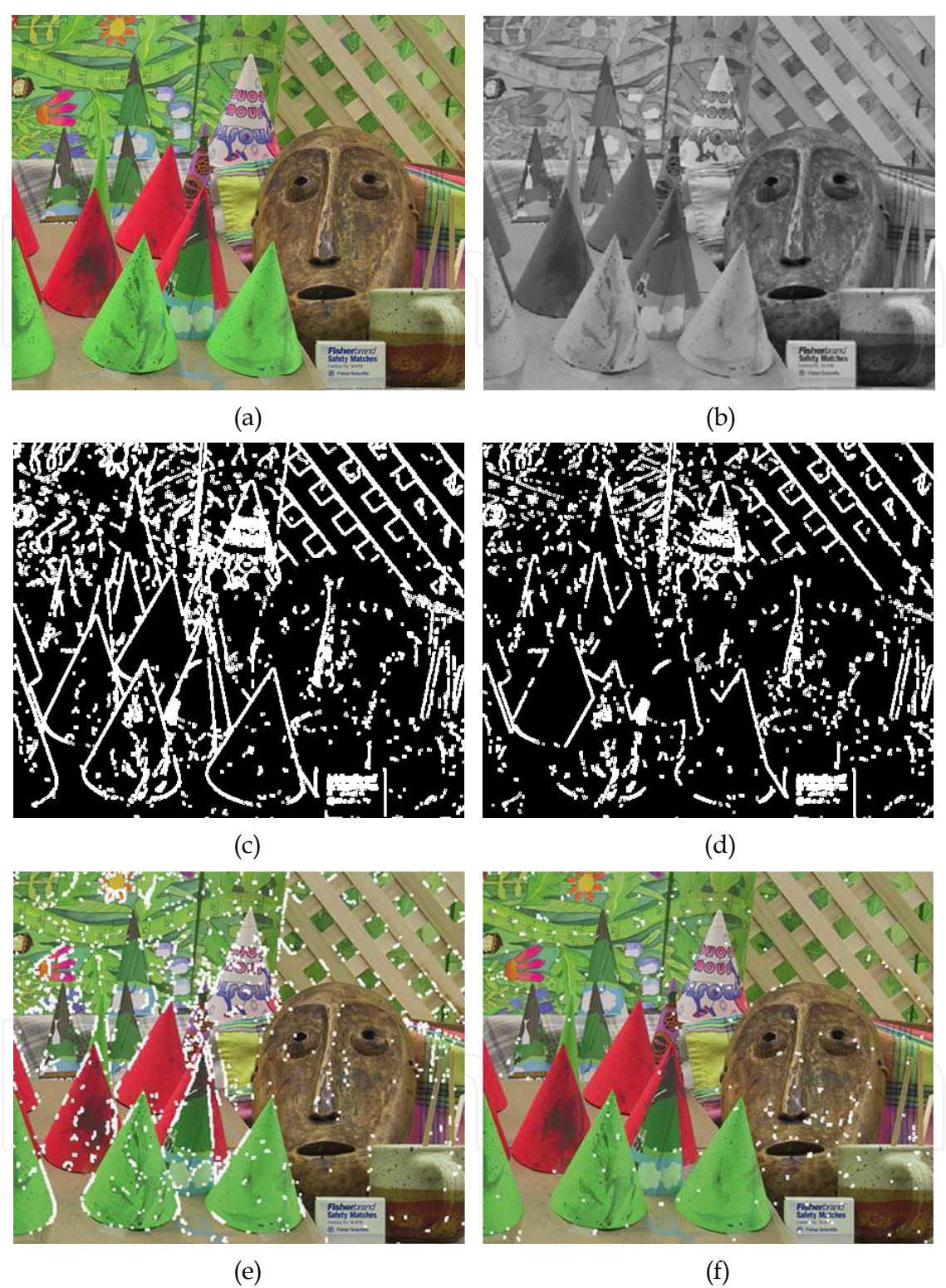
Fig. 7. Experimental results of color edges segmentation and gray level segmentation of Cones image of Middlebury database Scharstein & Szeliski (2002). (a) Color image. (b) The corresponding gray level image of (a). (c) Color-declivity image. (d) Declivity image. (e) Edge points extracted in color image but not in gray level image superimposed in white on color images. (f) Edge points extracted in gray level image but not in color image superimposed in white on color images.

| Image name | Number of | |
	declivities	color declivities
Barn 1	8446	12177
Cones	8538	12880
Teddy	8710	11733
Tsukuba	7216	10214

Table 1. Number of color declivities extracted in color images compared to number declivities extracted in corresponding gray level image

(a)   (b)

(c)   (d)

Fig. 8. Pixels of adjacent different colored objects with strictly monotonous gray level values. (a) color image. (b) color declivity image. (c) the corresponding gray level image of (a). (d) declivity image.
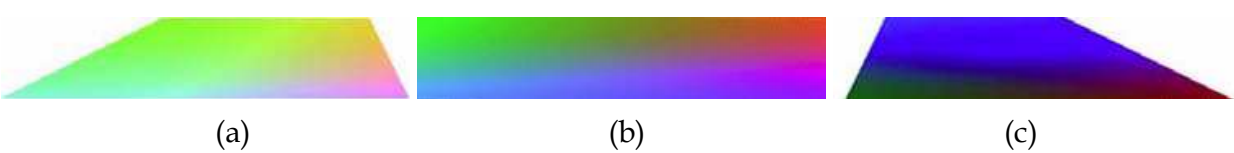

(a)   (b)   (c)

Fig. 9. Metamerism phenomena. Colors which reflect the same amount of light. Colors for gray level values equal to (a) 200, (b) 127 and (c) 50.

3. Color matching

3.1 State of the art
Introduction of different stereo correspondence algorithms can be found in the survey by *Scharstern* and *Szeliski* Scharstein & Szeliski (2002) and the one by *Brown et al.* Brown & Hager (2003). Matching approaches can be divided into *local* and *global* methods depending on their optimization strategy Brown & Hager (2003).

3.1.1 Local methods
Local methods can be very efficient but they are sensitive to locally ambiguous regions in images. They fall into three categories:
- Block matching Banks & Corke (2001): Search for maximum match score or minimum error over small region, typically using variants of cross-correlation or robust rank metrics. These methods are very suitable for dense matching and conceivable in real-time. We have a correct matching in the case of a light vertical displacement between

stereoscopic pair. These algorithms always provide a matching result even in the case of an occlusion which implicates a false matching. They are also little accurate on zones with not enough textures and sensitive to depth discontinuity.

- Gradient methods Twardowski et al. (2004): Minimize a functional, typically the sum of squared differences, over a small region. These methods has a correct matching in the case of a light vertical displacement between stereoscopic pair. They are little accurate on zones with few texture or too texture and sensitive to depth discontinuity. They give a poor results with scenes which have a large disparity.
- Feature matching Shen (2004): Match dependable features rather than intensities themselves. The quality of matching and the computation time depends on quality and computation time of detection algorithms of features.

3.1.2 Global methods

Global methods can be less sensitive to locally ambiguous regions in images, since global constraints provide additional support for regions difficult to match locally. They fall into six categories:

- Dynamic programming Bensrhair et al. (1996)Deng & Lin (2006): Determine the disparity surface for a scanline as the best path between two sequences of ordered primitives. Typically, order is defined by the epipolar ordering constraint. These methods have a good matching in the case of zones with not enough textures. They resolve the problems of the matching in the case of occlusions. Nevertheless, a light vertical displacement between stereoscopic pair misleads the matching. In the case of a local error of matching, this error is spread throughout the research line.
- Graph cuts Veksler (2007): Determine the disparity surface as the minimum cut of the maximum flow in a graph. The disparity map obtained with these methods is more accurate than that obtained by the dynamic programming. These methods have tendency to flatten objects on the disparity map. They consume too much computation time and as a result it is not possible to use them for real-time application.
- Intrinsic curves: Map epipolar scanlines to intrinsic curve space to convert the search problem to a nearest-neighbors lookup problem. Ambiguities are resolved using dynamic programming.
- Nonlinear diffusion: Aggregate support by applying a local diffusion process.
- Belief propagation: Solve for disparities via message passing in a belief network.
- Correspondenceless methods: Deform a model of the scene based on an objective function.

3.2 Color matching based on dynamic programming

The matching problem based on dynamic programming can be summarized as finding an optimal path on a two-dimensional graph whose vertical and horizontal axes respectively represent the color declivities of a left line and the color declivities of the stereo-corresponding right line. Axes intersections are nodes that represent hypothetical color-declivity associations. Optimal matches are obtained by the selection of the path which corresponds to a maximum value of a global gain. The matching algorithm consists of three steps:

Step 1. Taking into account a geometric constraint, all possible color-declivity associations $(R(i, l); L(j, l))$ are constructed. Let X_{cRi} be the position of the right color-declivity $R(i,$

l) in the line *l* of right image. Let X_{cLj} be the position of the left color-declivity $L(j, l)$ in the line *l* of left image. $(R(i, l); L(j, l))$ satisfies the geometric constraint if $0 < X_{cRi} - X_{cLj} < disp_{max}$. $disp_{max}$ is the maximum possible disparity value; it is adjusted according to the length of the baseline and the focal length of the cameras.

Step 2. Hypothetical color-declivity associations (constructed in step 1) which validate non-reversal constraint in color-declivity correspondence are positioned on the 2D graph. Each node in the graph (i.e. hypothetical color-declivity association) is associated to a local gain (see subsection 3.3) which represents the quality of the declivity association. As a result, we obtain several paths from an initial node to a final node in the graph. The gain of the path, i.e., the global gain, is the sum of the gains of its primitive paths. This gain is defined as follows. Let $G(e, f)$ be the maximum gain of the partial path from an initial node to node (e, f), and let $g(e, f, q, r)$ be the gain corresponding to the primitive path from node (e, f) to node (q, r), which in fact, only depends on node (q, r). Finally, $G(q, r)$ is computed as follows:

$$G(q,r) = \max_{(e,f)} \left[G(e,f) + g(e,f,q,r) \right] \tag{6}$$

Step 3. The optimal path in the graph is selected. It corresponds to the maximum value of the global gain. The best color-declivity associations are the nodes of the optimal path taking the uniqueness constraint into account. A disparity value $\delta(i, j, l)$ is computed for each color-declivity association $(R(i, l); L(j, l))$ of the optimal path of line *l*. $\delta(i, j, l)$ is equal to $X_{cLj} - X_{cRi}$, where X_{cRi} and X_{cLj} are the respective positions of $R(i, l)$ and $L(j, l)$ in the *l* right and *l* left epipolar lines. The result of color matching based on dynamic programming is a sparse disparity map.

3.3 Computation of local gain function

Computation of local gain associated to node in the 2D graph is based on photometric distance between two color declivities. Let X_{cRi} and X_{cLj} be the positions of two color declivities $R(i, l)$ and $L(j, l)$ respectively. Let $I_{R_c}(u_i - k)$ and $I_{L_c}(u_j - k)$ be the intensity of left neighbors of $R(i, l)$ and $L(j, l)$ respectively in color channel *c*, with $k = 0,1$ and 2 and $c = 1,2$ and 3. And, let $I_{R_c}(u_{i+1} + k)$ and $I_{L_c}(u_{j+1} + k)$ be the intensity of right neighbors of $R(i, l)$ and $L(j, l)$ respectively in color channel *c* with $k = 0,1$ and 2. Left and right photometric distances between $R(i, l)$ and $L(j, l)$ in channel *c* of color image are computed based on SAD (Sum of Absolute Differences):

$$l_{phdist_c} = \sum_{k=0}^{2} |I_{R_c}(u_i - k) - I_{L_c}(u_j - k)| \tag{7}$$

$$r_{phdist_c} = \sum_{k=0}^{2} |I_{R_c}(u_{i+1} + k) - I_{L_c}(u_{j+1} + k)| \tag{8}$$

Based on (7) and (8), local gain is computed. Classic methods tend to minimize a cost function. The main difficulty with this approach is that the cost value can increase indefinitely, which affects the computation time of the algorithm. Contrary to classic methods, the gain function is a non-linear function which varies between 0 and a maximum self-adaptive value equal to:

$$3 \times \max_{\forall \ m \in \Omega_{i,j}} (g_{max_c}) \tag{9}$$

with

$$g_{max_c} = 3 \times (d_{tR_c} + d_{tL_c}) \tag{10}$$

d_{tRc} and d_{tLc} are respectively the self-adaptive threshold value for the detection of relevant color declivities in right and left corresponding scan lines for channel number c. $\Omega_{i,j} = \Omega_i \cup \Omega_j$, where Ω_i and Ω_j are the sets (see subsection 2.2) associated respectively to color declivities $R(i, l)$ and $L(i, l)$. The gain function is calculated as follow:

<u>Case 1.</u>
if $\forall \ c \in \{1, 2,3\}$ ($l_{phdist_c} < g_{max_c}$ and $r_{phdist_c} < g_{max_c}$) then

$$gain = \frac{1}{Card(\Omega_{i,j})} \sum_{c \in \Omega_{i,j}} (3 \times g_{max_c} - l_{phdist_c} - r_{phdist_c}) \tag{11}$$

<u>Case 2.</u>
if $\forall \ c \in \{1, 2,3\}$ ($l_{phdist_c} < g_{max_c}$ and $r_{phdist_c} \geq g_{max_c}$) then

$$gain = \frac{1}{Card(\Omega_{i,j})} \sum_{c \in \Omega_{i,j}} (g_{max_c} - l_{phdist_c}) \tag{12}$$

<u>Case 3.</u>
if $\forall \ c \in \{1, 2,3\}$ ($l_{phdist_c} \_ g_{max_c}$ and $r_{phdist_c} < g_{max_c}$) then

$$gain = \frac{1}{Card(\Omega_{i,j})} \sum_{c \in \Omega_{i,j}} (g_{max_c} - r_{phdist_c}) \tag{13}$$

The gain function is computed
1. If there is a global (case 1), a left (case 2) or a right (case 3) color photometric similarity (i.e. a photometric similarity in each channel of color image). The gain function is computed to advantage global color photometric similarity compared to left or right similarity.
2. If monotonies of considered left and right color declivities are the same in each channel of $\Omega_{i,j}$. Due to different view of stereoscopic cameras, occlusions may occur. For example, background of left side of an object in left image may be occluded in right image. As a consequence, projections of a 3D point in color planes of the two cameras (declivities to be matched) may not be extracted in same channels. Then, $\Omega_{i,j}$ is equal to $\Omega_i \cup \Omega_j$. In the case of the example of occlusion, declivities to be matched have the same right photometric neighborhood. As a consequence, declivities in order to be matched must have the same monotony, otherwise it means that one of the edge point has not been extracted.

3.4 Experimental results and discussion
In Fig. 11, Fig. 12 and table 1 color matching is compared to gray level matching. The MARS/PRESCAN database van der Mark & Gavrila (2006) is used. It is composed of 326 pairs of synthetic color stereo images and ground truth data. Resolution of image is 256 x 256 pixels.

	MARS/PRESCAN database	
Image size	256 × 256 × 24 (color)	256 × 256 × 8 (gray level)
Number of frames	326	326
Mean of number of declivity associations	4503	3470
Mean computation time of edge extraction in a line of image (in ms)	0.12	0.04
Mean computation time of matching in a line of image (in ms)	0.12	0.12
Processor	Centrino 1.73 GHz	Centrino 1.73 GHz

Table 2. Computation time of color and gray level matching based on dynamic programming obtained from MARS/PRESCAN database which is composed of 326 stereo images.

(a)   (b)

(c)   (d)
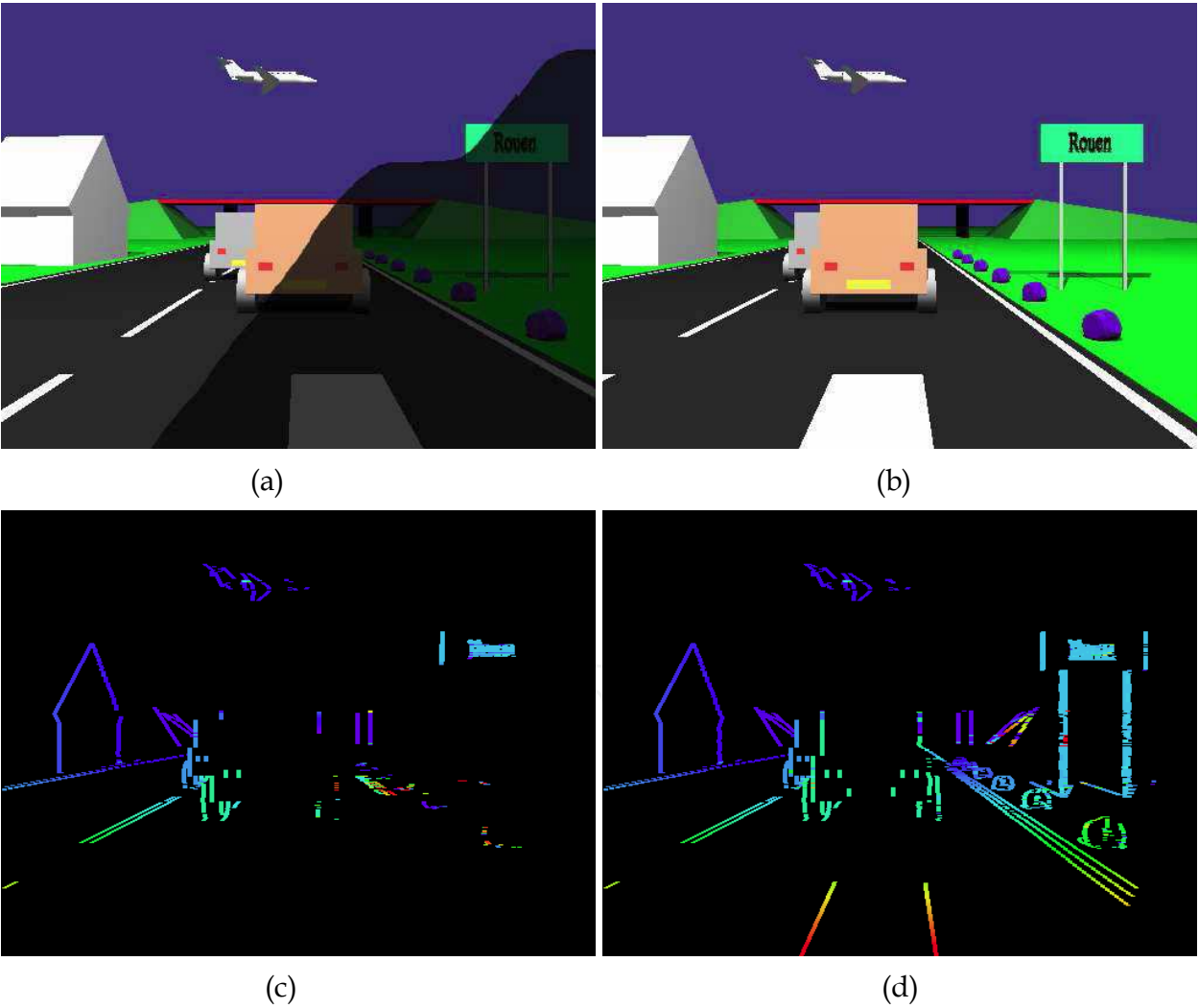
Fig. 10. Experimental results of disparity map construction. Disparity is coded with false color: hot color corresponds to close objects; cold color corresponds to far objects. (a) Left color syhntetic image with different contrast in the bottom-right region. (b) Right color syhntetic image. (c) Gray level matching. (d) Color matching.
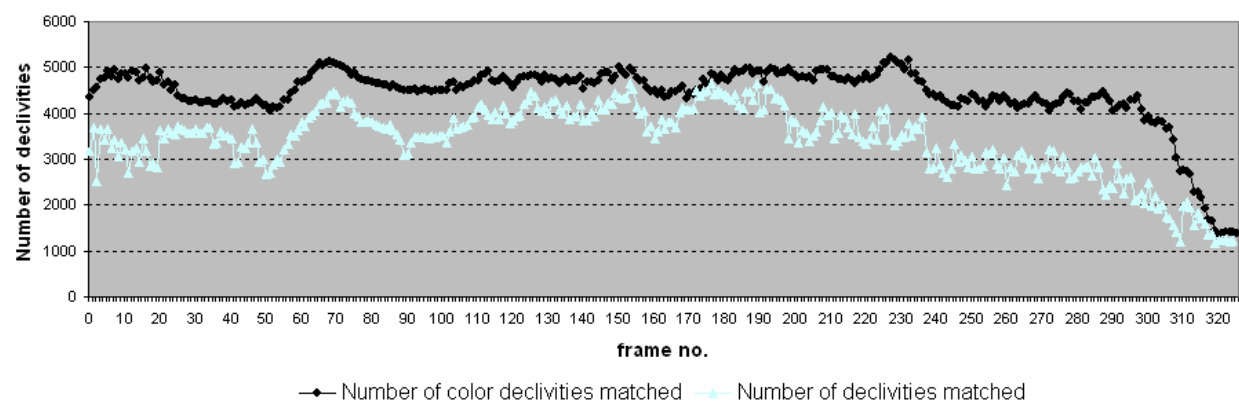
Fig. 11. Number of color declivity associations compared to gray level declivity associations obtained from MARS/PRESCAN database which is composed of 326 stereo images.
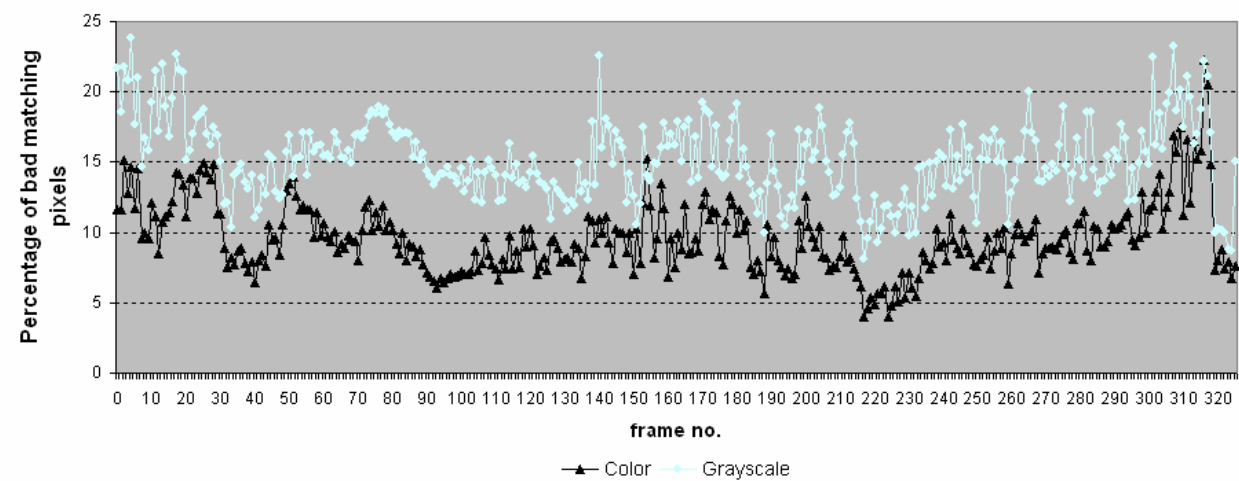

Fig. 12. Percentage of bad color matching compared to percentage of bad gray level matching obtained from MARS/PRESCAN database which is composed of 326 stereo images. These percentages have been computed based on (14).

Fig. 11 shows that the number of color association obtained from MARS/PRESCAN database is higher than the number of gray level association obtained from the gray level version of MARS/PRESCAN database. For this sequence, contribution of color corresponds to a 33% mean increase in the number of association with respect to the number of gray level association. The mean number of color declivities is 5700 for color image. The mean number of declivities is 5200 for gray level image. It corresponds to a 10% mean increase in the number

$$B = \frac{1}{100} \times \frac{1}{Card(\Lambda)} \sum_{k=1}^{Card(\Lambda)} \left(\left| \delta(x(k),y(k)) - \delta_{gt}(x(k),y(k)) \right| > \Delta \right) \qquad (14)$$

4. Obstacle detection

4.1 Ground plane estimation

In the previous sections we proved that color matching is more reliable than gray level matching in associating edge points. In this section we will show some of the consequences for a typical application of stereo vision in intelligent vehicles: ground plane estimation. Often, the v-disparity Labayrade et al. (2002) is used to estimate ground plane that allows to distinguish obstacles. The road surface of the synthetic images from MARS/PRESCAN database is flat van der Mark & Gavrila (2006). They, to detect road surface, the Hough transformation is used to detect only a single dominant line feature. This line is then compared to the line found by the same method in the ground truth disparity image. The difference in angle between the two lines shows how ground plane estimation is affected by the quality of the disparity image. For all images from test sequence, the differences in ground plane angle is shown on Fig. 13(a) for color process and on Fig. 13(b) for grayscale process. With the first third of the stereo pairs of database, the ground plane is detected without error. From frame number 188, we diagnose errors in the detection of the angle of ground plane. Using sparse 3D map computed with color process, We improve the perfect detection of ground plane of 10%.
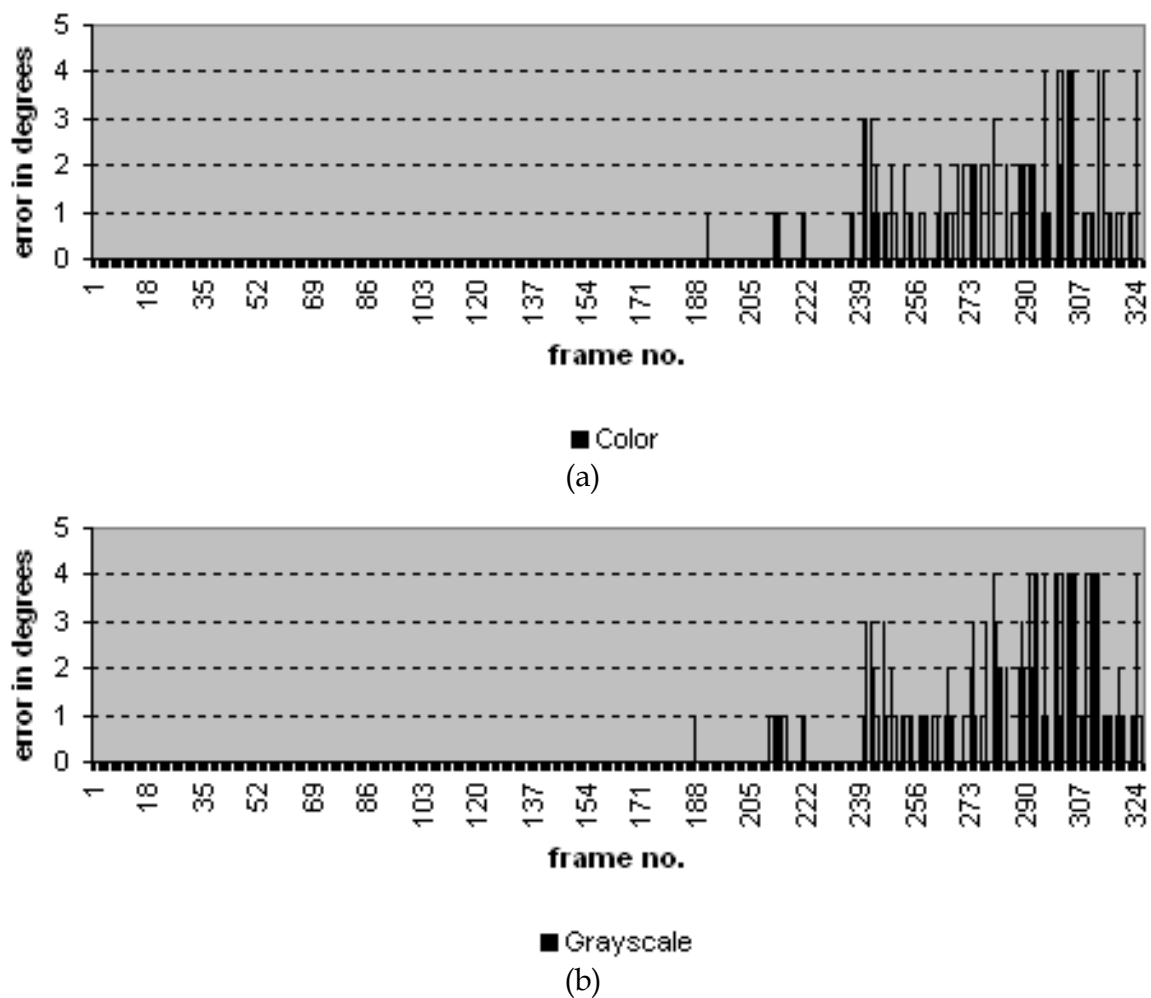

(a)

(b)

Fig. 13. Error in ground plane angle estimation based on V-disparity using (a) color matching process, (b) graylevel process to compute 3D Sparse Map

4.2 Extraction of 3D edges of obstacle

Within the framework of road obstacle detection, road features can be classified into two classes: *Non-obstacle* and *Obstacle*. An obstacle is defined as something that obstructs or may obstruct the intelligent vehicle driving path. Vehicles, pedestrians, animals, security guardrails are examples of Obstacles. Lane markings, artifacts are examples of Non-obstacles. In order to detect obstacles, our laboratory has conceived an operator which extracts 3D edges of obstacle from disparity map Toulminet et al. (2004) Cabani et al. (2006b) Cabani et al. (2006a) Toulminet et al. (2006). The extraction of the 3D edges of obstacles has been conceived as a cooperation of two methods:

- Method 1: this method selects 3D edges of obstacle by thresholding their disparity value; the threshold values are computed based on the detection of the road modeled by a plane. This method is sensitive to modeling and method used to detect the road (the v-disparity is used to detect road plane).
- Method 2: this method selects 3D straight segments by thresholding their inclination angle with respect to the road plane; 3D straight segments are constructed based on disparity map. This method does not suffer from approximate modeling and detection of the road. But, the extraction of 3D edges of obstacle is sensitive to noise in disparity measurement.

The cooperation of the two methods takes advantage of different sensitivity of the two methods in order to optimize robustness and reliability of the extraction of 3D edges of obstacle.

The output of the cooperation is a set of 3D points labeled as

- Edge of obstacle: extracted by the cooperation process or extracted by one of the two methods.
- Edge of non obstacle: not extracted.

4.3 Experimental results and discussion

In Fig. 14, the number of point of 3D edges of obstacle using color process is compared to number of point of 3D edges of obstacle using grayscale process obtained from MARS/PRESCAN database which is composed of 326 stereo images. Using color process, we succeed in extracting on average 20% of more points of 3D edges of obstacle. This contribution is very significant and is very important for a possible classification of obstacles in future works. The mean computation time for obstacle detection step is 31 ms. This important number of point of 3D edges of obstacle is owed in most cases in:

- Color declivity operator extract more relevant declivities (See subsection 2.4)
- Color matching is more robust in associating edge points (See subsection 3.4).
- For obstacle detection, method 1 depend on precision of plane road detection. In subsection 4.1, we prove that using 3D sparse map obtained with color process, the ground plane is detected more precisely.

Finally, we present in Fig. 15 an example of experimental results obtained on urban images acquired by our color stereo vision system Cabani et al. (2006a)Cabani et al. (2006b). The stereo vision system features 52 cm between the two optical centers and 8 mm of focal length of the lenses. Stereoscopic images have been acquired and registered on disc at the format of 768×574×24 bits at the rate of 5Hz (10 images per second). They have been processed at the format of 384×287×24 bits using a Pentium Centrino 1.73 GHz with 1 GByte memory using Windows XP. For sequences of Fig. 15, the stereo vision system was static.
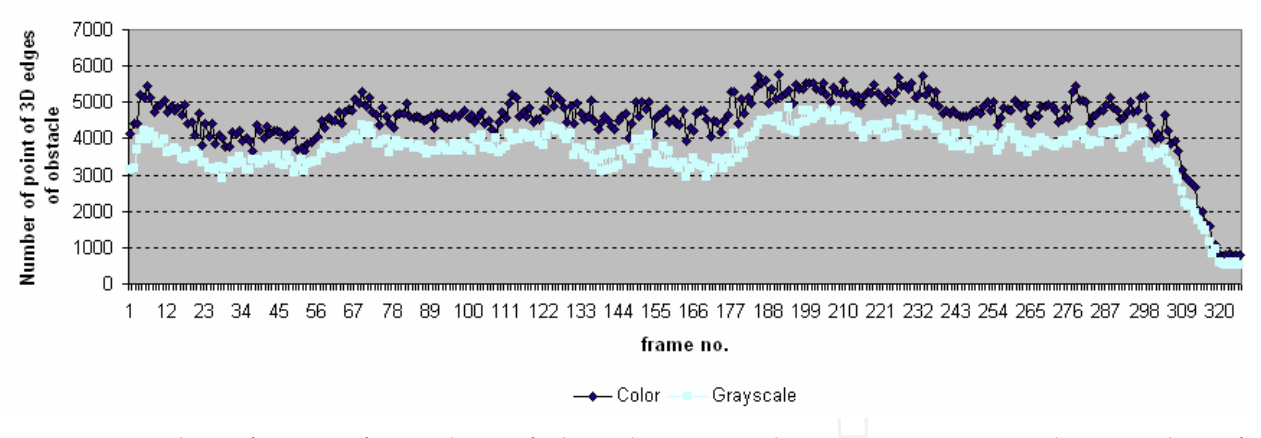
Fig. 14. Number of point of 3D edges of obstacle using color process compared to number of point of 3D edges of obstacle using grayscale process obtained from MARS/PRESCAN database which is composed of 326 stereo images.

edge extraction of both left and right images*	48 ms
color matching based on dynamic programming*	90 ms
obstacle detection	32 ms
Total computation time of extraction of 3D edges of obstacle	170 ms

*: these processes can be parallelized because the treatment is realized independently line by line.

Table 3. Computation time of obstacle detection on real road scene acquired by our color stereo vision system.

These stages have been acquired during daylight; they represent walking pedestrians and cars driving at low speed. In table 3, the mean computation time for each step of obstacle detection is presented. The total computation time of extraction of 3D edges of obstacle is equal to 170 ms. Therefore, our color stereo vision system works on quasi-real time (6 Hz).

5. Conclusion

In this paper, we have presented a color stereo vision-based approach for road obstacle detection. A self-adaptive color operator called color-declivity is presented. It extracts relevant edges in stereoscopic images. Edges are self-adaptively matched based on dynamic programming algorithm. Then, 3D edges of obstacle are extracted from constructed disparity map. These processes have been tested using Middlebury and MARS/PRESCAN databases. To test performance of the proposed approaches they have been compared to gray level-based ones and the improvement is highlighted.

Comparing the result obtained from the color stereo vision system to gray level stereo visions system initially conceived Bensrhair et al. (2002)Toulminet et al. (2006), we verified that more declivities are extracted and matched; and percentage of correct color matching is higher than the corresponding gray-level based matching. In addition, color matching is little sensitive to the intensity variation. Consequently, it is not necessary to obtain and maintain precise online color calibration.

Within the Driving Assistance Domain, color information presents an very important advantage. The extraction of ground plane is more accurate and the number of 3D edges of obstacles is more important.
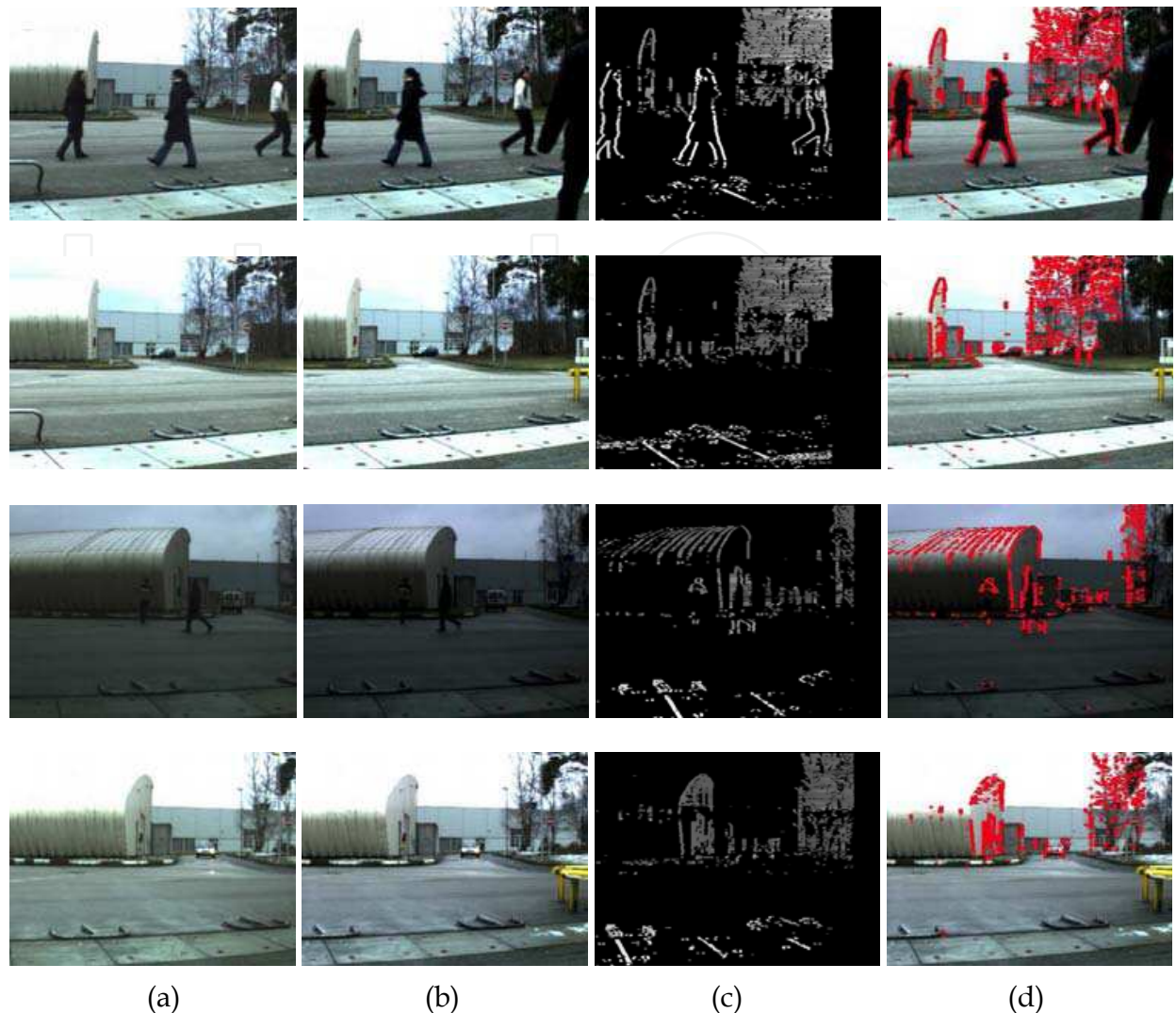
| | | | |
| (a) | (b) | (c) | (d) |

Fig. 15. Experimental results: (a) Leftt image. (b) Right image. (c) 3D sparse map obtained after the matching of color declivities using dynamic programming (d) 3D edges of obstacle superimposed in red on the right image.

Finally, color-based extraction of 3D edges of obstacle has been tested on real road scenes. It works on quasi-real time (6 Hz). The future work will focus to optimize computation time. In fact, extraction edges based on color declivity and color matching based on dynamic programming can be parallelized because these processes are executed line by line.

6. References

Alessandretti, G., Broggi, A. & Cerri, P. (2007). Vehicle and guard rail detection using radar and vision data fusion, *IEEE Transactions on Intelligent Transportation Systems* 8(1): 95– 105.

Banks, J. & Corke, P. (2001). Quantitative evaluation of matching methods and validity measures for stereo vision, *The International Journal of Robotics Research* 20(7): 512– 532. URL: *http://ijr.sagepub.com/cgi/content/abstract/20/7/512*

Bensrhair, A., Bertozzi, M., Broggi, A., Fascioli, A., Mousset, S. & Toulminet, G. (2002). Stereo vision-based feature extraction for vehicle detection, *Proceedings of the IEEE Intelligent Vehicles Symposium, Versailles, France.*

Bensrhair, A., Miché, P. & Debrie, R. (1996). Fast and automatic stereo vision matching algorithm based on dynamic programming method, *Pattern Recognition Letters* 17: 457– 466.

Bertozzi, M., Broggi, A., Caraffi, C., Del Rose, M., Felisa, M. & Vezzoni, G. (2007). Pedestrian detection by means of far-infrared stereo vision, *Computer Vision and Image Understanding* 106(2-3): 194–204.

Betke, M., Haritaoglu, E. & Davis, L. (2000). Real-time multiple vehicle detection and tracking from a moving vehicle, *Machine Vision and Applications* 12(2): 69–83.

Betke, M. & Nguyen, H. (1998). Highway scene analysis from a moving vehicle under reduced visibility conditions, *Proceedings of the IEEE Intelligent Vehicles Symposium, Stuttgart, Allemagne.*

Broggi, A., Fascioli, A., Carletti, M., Graf, T. & Meinecke, M. (2004). A multi-resolution approach for infrared vision-based pedestrian detection, *Proceedings of the IEEE Intelligent Vehicles Symposium, Parma, Italy.*

Brown, M. & Hager, G. (2003). Advances in computational stereo, *IEEE Transactions on Pattern Analysis and Machine Intelligence* 25(8): 993–1008.

Cabani, I., Toulminet, G. & Bensrhair, A. (2005). Color-based detection of vehicle lights, *Proceedings of IEEE intelligent Vehicle Symposium, Las Vegas, USA.*

Cabani, I., Toulminet, G. & Bensrhair, A. (2006a). A color stereo vision system for extraction of 3d edges of obstacle, *Proceedings of the IEEE International Conference on Intelligent Transportation Systems*, Toronto, Canada.

Cabani, I., Toulminet, G. & Bensrhair, A. (2006b). Color stereoscopic steps for road obstacle detection, *The 32nd Annual Conference of the IEEE Industrial Electronics Society, IECON'06*, Paris, France.

Canny, J. (1986). A computational approach to edge detection, *IEEE Transactions on Pattern Analysis and Machine Intelligence* 8(6): 679–698.

Carron, T. & Lambert, P. (1994). Color edge detector using jointly hue, saturation and intensity, *Proceedings of the IEEE International Conference on Image Processing*, Vol. 3, pp. 977–981.

Carron, T. & Lambert, P. (1995). Fuzzy color edge extraction by inference rules quantitative study and evaluation of performances, *Proceedings of the IEEE International Conference on Image Processing*, Vol. 2, pp. 181–184.

Chapron, M. (1992). A new chromatic edge detector used for color image segmentation, *Proceedings of the IEEE International Conference on Pattern Recognition*, Vol. 3, pp. 311–314.

Chapron, M. (1997). A chromatic contour detector based on abrupt change techniques, *Proceedings of the IEEE International Conference on Image Processing*, Vol. 3, Santa Barbara, CA, pp. 18–21.

Chapron, M. (2000). A color edge detector based on dempster-shafer theory, *Proceedings of the IEEE International Conference on Image Processing*, Vol. 2, pp. 812–815.

Cheng, H.-Y., Jeng, B.-S., Tseng, P.-T. & Fan, K.-C. (2006). Lane detection with moving vehicles in the traffic scenes, *IEEE Transactions on Intelligent Transportation Systems* 7(4): 571– 582.

Cheng, H., Zheng, N., Zhang, X. & van deWetering, H. (2007). Interactive road situation analysis for driver assistance and safety warning systems: Framework and algorithms, *IEEE Transactions on Intelligent Transportation Systems* 8(1): 157–167.

Cumani, A. (1991). *Edge detection in multispectral images, Comput. Vis. Graph. Image Process.: Graphical Models Image Processing* 53(1): 40–51.

Deng, Y. & Lin, X. (2006). A fast line segment based dense stereo algorithm using tree dynamic programming, *Proceedings of the European Conference on Computer Vision*, Vol. 3953/2006, Springer Berlin / Heidelberg, pp. 201–212.

Di-Zenzo, S. (1986). A note on the gradient of a multi-image, *Computer Vision, Graphics and Image Processing* 33(1): 116–125.

Djuric, P. & Fwu, J. (1997). On the detection of edges in vector images, *IEEE Transactions on Image Processing* 6(11): 1595–1601.

Fan, J., Aref,W. G., Hacid, M.-S. & Elmagarmid, A. K. (2001). An improved automatic isotropic color edge detection technique, *Pattern Recognition Letters* 22(13): 1419–1429.

Fan, J., Yau, D., Elmagarmid, A. & Aref, W. (2001). Automatic image segmentation by integrating color-edge extraction and seeded region growing, *IEEE Transactions on Image Processing* 10(10): 1454–1466.

Franke, U. (2000). Real-time stereo vision for urban traffic scene understanding, *Proc. of the IEEE Intelligent Vehicles Symp., Dearborn, USA.*

Franke, U., Gavrila, D., Gorzig, S., Lindner, F., Paetzold, F. & Wohler, C. (1999). Autonomous driving goes downtown, *IEEE Intelligent Systems* 13(6): 40–48.

Gao, B. & Coifman, B. (2006). Vehicle identification and gps error detection from a lidar equipped probe vehicle, *Proceedings of the IEEE International Conference on Intelligent Transportation Systems*, pp. 1537–1542.

Gern, A., Franke, U. & Levi, P. (2000). Advanced lane recognition - fusing vision and radar, *Proc. of the IEEE Intelligent Vehicles Symp., Dearborn, USA.*

Heddley, M. & Yan, H. (1992). Segmentation of color images using spatial and color space information, *Journal Electron. Imag.* 1(4): 374–380.

Hueckel, M. H. (1971). An operator which locates edges in digitized pictures, *J. ACM* 18(1): 113–125.

Huntsberger, T. & Descalzi, M. (1985). Color edge detection, *Pattern Recognition Letters* 3(3): 205–209.

Jia, Z., Balasuriya, A. & Challa, S. (2007). Vision based data fusion for autonomous vehicles target tracking using interacting multiple dynamic models, *Computer Vision and Image Understanding, In Press, Corrected Proof* .

Kogler, J., Hemetsberger, H., Alefs, B., Kubinger, W. & Travis, W. (2006). Embedded stereo vision system for intelligent autonomous vehicles, *Proceedings of the IEEE Intelligent Vehicles Symposium*, pp. 64–69.

Kruse, F., Follster, F. & Ahrholdt, M. (2004). Target classification based on near-distance radar sensor, *Proc. of the IEEE Intelligent Vehicles Symp., Parma, Italy.*

Labayrade, R., Aubert, D. & Tarel, J. (2002). Real time obstacle detection in stereovision on non flat road geometry through v-disparity representation, *Proc. of the IEEE Intelligent Vehicles Symp., Versailles, France.*

Lombardi, P. & Zavidovique, B. (2004). A context-dependent vision system for pedestrian detection, *Proceedings of the IEEE Intelligent Vehicles Symposium, Parma, Italy.*

Macaire, L. (2004). *Exploitation de la couleur pour la segmentation et l'analyse d'images*, PhD thesis, (HDR), Universit´e des Sciences et Technologies de Lille.

Macaire, L., Ultre, V. & Postaire, J. (1996). Determination of compatibility coefficients for color edge detection by relaxation, *Proceedings of the IEEE International Conference on Image Processing*, Vol. 3, pp. 1045–1048.

Machuca, R. & Phillips, K. (1983). Applications of vector fields to image processing, *IEEE Transactions on Pattern Analysis and Machine Intelligence* 5(3): 316–329.

Maldonado-Bascon, S., Lafuente-Arroyo, S., Gil-Jimenez, P., Gomez-Moreno, H. & Lopez-Ferreras, F. (2007). Road-sign detection and recognition based on support vector machines, *IEEE Transactions on Intelligent Transportation Systems* 8(2): 264–278.

Malowany, M. & Malowany, A. (1989). Color edge detectors for a vlsi convolver, *in* W. Pearlman (ed.), *Proc. SPIE Vol. 1199, p. 1116-1126, Visual Communications and Image Processing IV, William A. Pearlman; Ed.,* Vol. 1199 of *Presented at the Society of Photo-Optical Instrumentation Engineers (SPIE) Conference*, pp. 1116–1126.

Miché, P. & Debrie, R. (1995). Fast and self-adaptive image segmentation using extended declivity, *Annals of telecommunication* 50(3-4): 401–410.

Möbus, R. & Kolbe, U. (2004). Multi-target multi-object tracking, sensor fusion of radar and infrared, *Proceedings of the IEEE Intelligent Vehicles Symposium, Parma, Italy.*

Moghaddamzadeh, A. & Bourbakis, N. (1995). A fuzzy approach for smoothing and edge detection in color images, *In Proceedings of the SPIE*, Vol. 2421, pp. 90–102.

Moghaddamzadeh, A., Goldman, D. & Bourbakis, N. (1998). Fuzzy-like approach for smoothing and edge detection in color images, *International Journal of Pattern Recognition and Artificial Intelligence* 12(6): 801–816.

Nevatia, R. (1977). A color edge detector and its use in scene segmentation, *IEEE Trans. Syst., Man, Cybern.* 7: 820–826. *PathFindIR* (n.d.). URL: *www.flir.com*

Peli, T. & Malah, D. (1982). A study of edge detection algorithms, *Computer Graphics and Image Processing* 20: 1–21.

Pietikainen, M. & Harwood, D. (1986). Edge information in color images based on histograms of differences, *Proceedings of the IEEE International Conference on Pattern Recognition*, Paris, France, pp. 594–596.

Pratt,W. (1977). *Digital Image Processing,*Wiley, New York.

Ruzon, M. & Tomasi, C. (2001). Edge, junction, and corner detection using color distributions, *IEEE Transactions on Pattern Analysis and Machine Intelligence* 23(11): 1281–1295.

Salinas, R., Richardson, C., Abidi, M. & Gonzalez, R. (1996). Data fusion: color edge detection and surface reconstruction through regularization, *IEEE Transactions on Industrial Electronics* 43(3): 355–363.

Sankur, B. & Sezgin, M. (2004). Survey Over Image Thresholding Techniques and Quantitative Performance Evaluation, *Journal of Electronic Imaging* 13(1): 146–165.

Scharcanski, J. & Venetsanopoulos, A. (1997). Edge detection of color images using directional operators, *IEEE Transactions on Circuits and Systems for Video Technology* 7(2): 397–401.

Scharstein, D. & Szeliski, R. (2002). A taxonomy and evaluation of dense twoframe stereo correspondence algorithms, *International Journal of Computer Vision, www.middlebury.edu/stereo/* 47: 7–42.

Shen, D. (2004). Image registration by hierarchical matching of local spatial intensity histograms., *Medical Image Computing and Computer-Assisted Intervention*, Vol. 3216/2004, Springer Berlin/Heidelberg, pp. 582–590.

Shiozaki, A. (1986). Edge extraction using entropy operator, *Computer Vision, Graphics and Image Processing* 36(1): 1–9.

Steux, B., Laurgeau, C., Salesse, L. & Wautier, D. (2002). Fade : A vehicle detection and tracking system featuring monocular color vision and radar data fusion, *Proceedings of the IEEE Intelligent Vehicles Symposium, Versailles, France*.

Tao, H.&Huang, T. (1997). Color image edge detection using cluster analysis, *Proceedings of the IEEE International Conference on Image Processing*, Vol. 1, Washington, D.C., pp. 834– 837.

Toulminet, G., Bertozzi, M., Mousset, S., Bensrhair, A. & Broggi, A. (2006). Vehicle detection by means of stereo vision-based obstacles features extraction and monocular pattern analysis, *IEEE Transactions on Image Processing* 15(8): 2364–2375.

Toulminet, G., Mousset, S. & Bensrhair, A. (2004). Fast and accurate stereo vision-based estimation of 3-d position and axial motion of road obstacles, *International Journal of Image and Graphics, Special Issue on 3D Object Recognition* 4(1): 99–126.

Trahanias, P. & Venetsanopoulos, A. (1996). Vector order statistics operators as color edge detectors, *IEEE Transactions on Systems, Man, and Cybernetics* 26(1): 135–143.

Tsang, P. & Tsang,W. (1996). Edge detection on object color, *Proceedings of the IEEE International Conference on Image Processing*, Vol. 3, pp. 1049–1052.

Tsang, W. H. & Tsang, P. W. M. (1997). Suppression of false edge detection due to specular reflection in color images, *Pattern Recognition Letters* 18(2): 165–171.

Twardowski, T., Cyganek, B. & Borgosz, J. (2004). Gradient based dense stereo matching., *International Conference of Image Analysis and Recognition*, pp. 721–728.

van der Mark, W. & Gavrila, D. (2006). Real-time dense stereo for intelligent vehicles, *IEEE Transactions on Intelligent Transportation Systems*, Vol. 7, pp. 38–50.

Veksler, O. (2007). Graph cut based optimization for mrfs with truncated convex priors, *Proceedings of the IEEE Computer Society Conference on Computer Vision and Pattern Recognition*.

Weeks, A., Felix, C. & Myler, H. (1995). Edge detection of color images using the hsl color space, *in* E. R. Dougherty, J. T. Astola, H. G. Longbotham, N. M. Nasrabadi & A. K. Katsaggelos (eds), *Proc. SPIE Vol. 2424, p. 291-301, Nonlinear Image Processing VI*, Vol. 2424 of *Presented at the Society of Photo-Optical Instrumentation Engineers (SPIE) Conference*, pp. 291–301.

Wen, F., Hu, M. & Yuan, B. (2002). A comparative study on color edge detection, *In Proc. IEEE Region 10 Conf. Comput., Commun., Contr. Power Eng.*, Vol. 1, pp. 511–514.

Woodfill, J. I., Buck, R., Jurasek, D., Gordon, G. & Brown, T. (2007). 3d vision: Developing an embedded stereo-vision system, *Computer* 40(5): 106–108.

Xu, F. & Fujimura, K. (2002). Pedestrian detection and tracking with night vision, *Proceedings of the IEEE Intelligent Vehicles Symposium, Versailles, France*.

Yang, C. & Tsai, W. (1996). Reduction of color space dimensionality by moment-preserving thresholding and its application for edge-detection in color images, *Pattern Recognition Letters* 17(5): 481–490.

Zhu, Y., Comaniciu, D., Pellkofer, M. & Koehler, T. (2006). Reliable detection of overtaking vehicles using robust information fusion, *IEEE Transactions on Intelligent Transportation Systems* 7(4): 401–414.

Zugaj, D. & Lattuati, V. (1998). A new approach of color images segmentation based on fusing region and edge segmentations outputs, *Pattern Recognition* 31(2): 105–113.
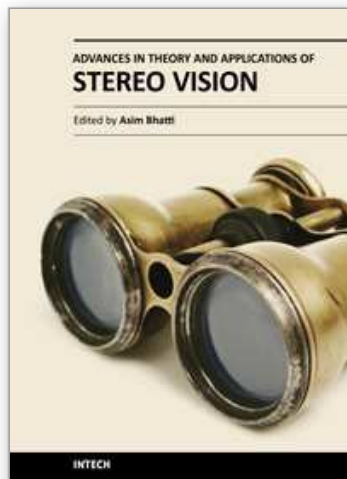
Advances in Theory and Applications of Stereo Vision

Edited by Dr Asim Bhatti

The book presents a wide range of innovative research ideas and current trends in stereo vision. The topics covered in this book encapsulate research trends from fundamental theoretical aspects of robust stereo correspondence estimation to the establishment of novel and robust algorithms as well as applications in a wide range of disciplines. Particularly interesting theoretical trends presented in this book involve the exploitation of the evolutionary approach, wavelets and multiwavelet theories, Markov random fields and fuzzy sets in addressing the correspondence estimation problem. Novel algorithms utilizing inspiration from biological systems (such as the silicon retina imager and fish eye) and nature (through the exploitation of the refractive index of liquids) make this book an interesting compilation of current research ideas.

How to reference

In order to correctly reference this scholarly work, feel free to copy and paste the following:

Iyadh Cabani, Gwenaelle Toulminet and Abdelaziz Bensrhair (2011). New Robust Obstacle Detection System Using Color Stereo Vision, Advances in Theory and Applications of Stereo Vision, Dr Asim Bhatti (Ed.), ISBN: 978-953-307-516-7, InTech, Available from: http://www.intechopen.com/books/advances-in-theory-and-applications-of-stereo-vision/new-robust-obstacle-detection-system-using-color-stereo-vision

INTECH
open science | open minds